Propagation at Extremely Low Frequencies

Dana Porrat and Antony C. Fraser-Smith

STAR Laboratory
Electrical Engineering Department
Stanford University
Stanford, CA 94305
USA

February 10, 2003

Contents

Extremely-low frequency (ELF) electromagnetic waves (frequencies in the range 3 Hz to 3 kHz) are of interest in the sciences and in communications for a number of reasons. Perhaps most important, lightning is a powerful natural source of electromagnetic radiation in this frequency range and the characteristics of lightning can be studied in considerable detail by making measurements on the waves it generates. In a communications context, the naturally-occurring lightning-generated waves constitute a noise background that can degrade an ELF communications link. On the other hand, ELF waves travel with little attenuation to large distances in the space between the earth's surface and the ionized upper layers of the earth's atmosphere (i.e., the ionosphere) and thus they can provide communications over large regions of the earth. Furthermore, when compared with the other higher-frequency forms of electromagnetic waves used for communications, ELF waves are relatively unaffected by disturbances in the ionosphere and thus they can provide a more reliable communications link during times of high solar activity. Finally, they penetrate quite well through the conducting materials typically encountered on the earth's surface and thus they can be used for probing the surface, for prospecting, and for certain forms of communication through the earth and the sea.

In this article, we provide a brief description of the propagation characteristics of these waves based on a simplified model of ELF electromagnetic wave propagation in the earth-ionosphere waveguide. We discuss some interesting consequences of the long-distance propagation of ELF waves through the waveguide, one of which is the focusing of the waves at the antipode of the source. Another is the occurrence of resonance in the waveguide. We also discuss some practical applications of ELF waves and the special considerations which can affect communication systems.

In order to better understand ELF wave propagation in the earth-ionosphere waveguide, the electrical properties of the waveguide walls need to be taken into account, as well as the effect of dynamic changes in the ionosphere. Another factor affecting the waveguide is the geomagnetic field, which causes the waveguide to be anisotropic. Finally, because the complexity of the waveguide makes its analytical description difficult, we discuss the two most common methods

for calculating the solution to particular ELF wave propagation problems.

1 Simplified Waveguide Model

A simple approximation of the earth–ionosphere waveguide, which is nonetheless useful in many situations, is the flat earth model. The waveguide is modeled as an infinite parallel plate waveguide with the curvature of the earth and the ionosphere neglected. Figure 1 presents the geometry with a cylindrical coordinate system (ρ, ϕ, z). The ground plane is located at $z = 0$ and the ionospheric boundary is at $z = h$.

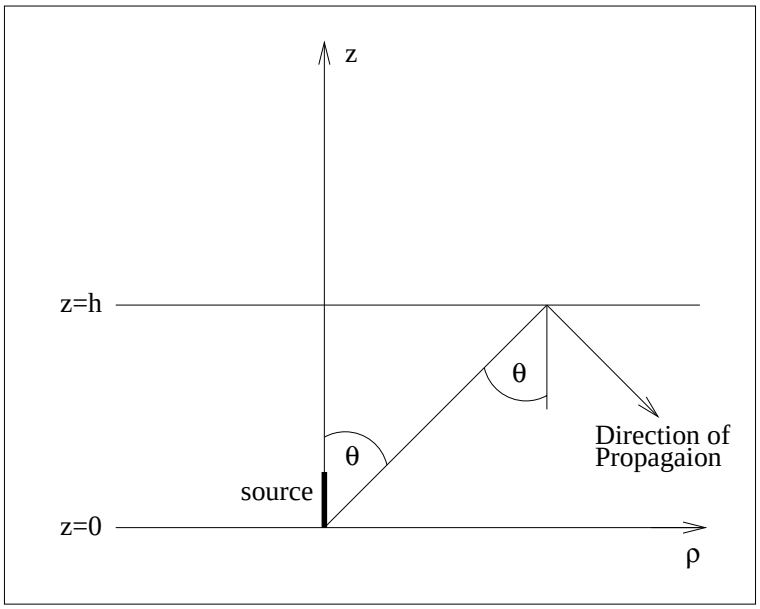

Figure 1: Geometry of the flat earth–ionosphere waveguide with a cylindrical coordinate system.

This model is valid for distances of up to half an earth radius from the source, because at greater distances the curvature of the earth affects ELF propagation.

The walls of the waveguide are modeled as perfect conductors, because in the ELF range, both the earth and the ionosphere have very high conductivities.

The vertical component of the electric field generated by a vertical electric

dipole of moment Ids, placed on the ground at the point (ρ=0, $z = 0$) in a flat waveguide with perfectly conducting walls, is described by Wait [87] as a modal series:

$$E_z = E_0 \frac{(\rho/\lambda)^{1/2}}{(h/\lambda)} e^{i[k\rho - \pi/4]} \sum_{n=0}^{\infty} \delta_n S_n^{3/2} e^{-ikS_n\rho} \cos(kC_n z) \qquad (1)$$

where

λ is the free space wavelength,

$k = \frac{2\pi}{\lambda}$,

$\eta = \sqrt{\mu_0/\epsilon_0} \simeq 120\pi\ \Omega$ is the free space impedance,

$E_0 = -i\frac{\eta Ids}{\lambda}\frac{e^{-ik\rho}}{\rho}$,

$\delta_n \cong \begin{cases} \frac{1}{2} & n = 0 \\ 1 & n = 1, 2, \ldots \end{cases}$

$S_n = \sin\theta_n = \sqrt{1 - C_n^{1/2}}$ is the sine of the eigenangle of the n^{th} mode (which may be complex),

$C_n = \cos\theta_n$ is the cosine of the eigenangle of the n^{th} mode,

and θ_n is the eigenangle of the nth mode.

Equation (1) describes the field measured within the waveguide, for $0 < z < h$. It is a far field approximation, valid at big enough distances from the source ($h \ll \rho$ and $\lambda \ll \rho$) where $\rho > 300$ km can be taken as a lower limit. See Bannister [9] for a development of field expressions at shorter distances from the source. The time dependence is $e^{i\omega t}$, where $\omega = \frac{2\pi c}{\lambda}$ is the angular frequency.

The other field components, in addition to E_z (eq. 1) can be calculated using Maxwell's equations and they are described by:

$$H_\phi = \frac{E_0}{\eta}\frac{(\rho/\lambda)^{1/2}}{(h/\lambda)} e^{i[k\rho - \pi/4]} \sum_{n=0}^{\infty} \delta_n S_n^{1/2} e^{-ikS_n\rho} \cos(kC_n z) \qquad (2)$$

$$E_\rho = E_\phi = H_z = H_\rho = 0 \qquad (3)$$

The modal phase velocity is $c/Re[S_n]$ and the modal attenuation factor is $-kIm[S_n]$ per unit distance.

The eigenangle θ_n can be interpreted as the incidence angle of the wavefront on the ionosphere, as indicated in figure 1. This interpretation of the eigenangle is closely related to the ray theory description of electromagnetic wave propagation in the waveguide, which is an alternative to the modal theory

discussed here. However, the ray theory treatment of the waveguide is of little consequence in the ELF band, so it is not discussed further.

The modes generated by the vertical dipole are all transverse magnetic (TM) modes, since the magnetic field is transverse to the direction of propagation of the wave as it propagates away from the source (and thus H_ρ=0).

Nickolaenko and Hayakawa [55] calculate the spectrum in the ELF band of the vertical electric field generated by a vertical dipole, computed from expressions based on the modal series, and demonstrate the Schumann resonance, a phenomenon which will shortly be described.

A horizontal electric dipole source of moment Ids, placed at ($z = z_0$, ρ=0) parallel to the $\phi = 0$ direction, generates a magnetic field whose vertical component is

$$H_z = -\frac{\sin\phi}{\eta} E_0 \frac{(\rho/\lambda)^{1/2}}{(h/\lambda)} \frac{e^{i[k\rho-\pi/4]}}{2} \sum_{m=1}^{\infty} S_m^{1/2} \sin(kC_m z_0) \sin(kC_m z) e^{-ikS_m\rho} \quad (4)$$

where

$S_m = \sin\theta_m = \sqrt{1 - C_m^2}$ is the sine of the eigenangle of the m^{th} mode,

$C_m = \cos\theta_m$ is the cosine of the eigenangle of the m^{th} mode,

and θ_m is the eigenangle of the mth mode.

Equation (4) is an approximation which is valid for $0 \leq z < h$, $h \ll \rho$ and $\lambda \ll \rho$, where $\rho > 300$ km can be taken as a lower limit for its validity. The time dependence is $e^{i\omega t}$. The other components of the field are zero, except for E_ϕ.

The modes generated by the horizontal dipole in the broadside direction are transverse electric (TE) modes, since the electric field is transverse to the direction of propagation of the wave (and thus E_ρ=0). In other directions, the horizontal dipole generates a mixture of TM and TE modes. The TE waves are weak at low altitudes (near the ground), because the horizontal electric field is extinguished near the conductive earth. Since most measurements of ELF fields are made by antennas mounted on the ground, the TE component they receive is weak. This is possibly the reason that the TE modes receive little attention in the scientific literature.

The modal equations (5) and (6) of the simple flat earth model with perfectly

conducting walls determine the eigenangles of the waveguide.

$$e^{-i2khC_n} = e^{-i2\pi n} \qquad n = 0, 1, 2, \ldots \tag{5}$$

$$e^{-i2khC_m} = e^{-i2\pi m} \qquad m = 1, 2, \ldots \tag{6}$$

For the TM and TE modes respectively.

The eigenangles for the TM mode are:

$$C_n = n\frac{\lambda}{2h} \quad n = 0, 1, \ldots \tag{7}$$

and for the TE modes:

$$C_m = m\frac{\lambda}{2h} \quad m = 1, 2, \ldots \tag{8}$$

The lowest TM mode is the 0^{th}, which propagates over the whole frequency range. This mode is also called the Transverse Electro–Magnetic (TEM) mode, because both the electric and the magnetic fields are transverse to the direction of propagation. The electric field is vertical (E_z component only), and the magnetic field is in the ϕ direction.

The higher modes, namely the TM modes with $n = 1, 2, \ldots$ and all the TE modes, propagate above a certain frequency, called the cutoff frequency, which characterizes each mode. The cutoff frequency of high order modes is higher than that of the lower order modes. Only the 1^{st} mode is of interest in the ELF range, because the cutoff frequencies for all the higher modes are above 3 kHz.

The cutoff frequency of these 1^{st} modes (TM and TE) varies between 1.5 kHz and 4 kHz depending on the height of the ionosphere.

When extending the waveguide model from the simple flat, perfectly conducting plate model, the following features may be considered:

- The reflections coefficients of the earth and the ionosphere
- The waveguide geometry
- The presence of the geomagnetic static field

The effects of these features of the waveguide on the ELF waves propagating within it are discussed in section 5.

2 Applications

ELF waves propagating in the earth–ionosphere waveguide undergo very low attenuation (sometimes as low as 1-2 dB/Mm). This allows ELF transmissions to propagate great distances, making this frequency range suitable for communication networks encompassing the whole globe. Bannister [8] discusses the attenuation in the ELF band and shows measurements of the attenuation rate at different frequencies.

Another important feature of ELF wave propagation is their good penetration into the earth and sea water. The skin depth, which characterizes penetration of electromagnetic waves into lossy materials, depends inversely on the square root of the wave frequency ($\delta \sim 1/\sqrt{\omega}$). Thus, ELF waves have a larger skin depth compared to waves in higher frequency bands and they penetrate better into conducting materials. For example, the skin depth of waves propagating at 70 Hz in sea water is 30.1 m. The comparatively large skin depth is the reason for operating submarine communication systems in the ELF range. An example of such a system is the United States' Navy ELF Communications System for communication with submarines, operating in the frequency range of 70–80 Hz. This system consists of two synchronous transmitters connected to 22.5 km quasi-orthogonal antennas.

The major difficulties when communicating in the ELF range are the need for large antennas and the low data rate. In order to achieve efficient transmission the physical dimensions of the antennas should be comparable to the wavelength of the communication frequency, so the long wavelengths inherent in the ELF range (100 km at 3 kHz up to 100,000 km at 3 Hz) make efficient antenna installation very difficult. This is a problem mainly in the transmitters, since on the receiving side the antenna/pre-amplifier combination is only limited by atmospheric noise in the frequency range of interest.

The useful bandwidth in an ELF communication system is limited by the low carrier frequency. Communication systems in the ELF range typically transmit at very low data rates compared to systems utilizing other frequency bands.

The large antenna dimensions needed for efficient transmission, and the in-

herent low bandwidth are the reasons that ELF communication systems are few and are usually run by governments for limited military usage.

Kelly [45] surveys engineering issues related to ELF systems, namely modulation, dispersion, antennas and system performance and coverage predictions.

2.1 Electrojet Modulation

A scientific application in the ELF band consists of the modulation of ionospheric currents, in particular the auroral electrojet. The auroral electrojet is an intense westward current, flowing in the D and E regions of the ionosphere (section 7 discusses the ionospheric layers). It flows within the auroral belt, a narrow oval–shaped region encircling the northern geomagnetic pole (a similar belt exists around the southern pole).

The intensity of the auroral electrojet is affected by the conductivity of the ionospheric D and E layers. Changes in the ionospheric conductivity can be artificially induced by heating the ionosphere with radio waves of appropriate frequency in the HF band, which are efficiently absorbed in the D and E layers. Amplitude–modulated heating of the D and E layers translates into amplitude–modulated conductivity of the medium, which modulates the intensity of the electrojet. The modulated electrojet re-radiates into the earth–ionosphere waveguide at the modulation frequency. Villaseñor et al. [83] study different modulation methods and polarizations of the heating wave, and Barr and Stubbe [13] discuss the radiation mechanism and evaluate the intensity of the radiated wave. Papadopoulos et al. [61] discuss the efficiency of the ELF/VLF generation process.

Generation of ELF/VLF signals by modulation of the auroral electrojet has been demonstrated in various ionospheric heating facilities. Experiments of this kind are discussed by Stubbe et al. [81], Ferraro et al. [22], Barr et al. [14], Rietveld at el. [74] and Barr et al. [12].

3 Background Noise

The sources of noise in the ELF range are lightning discharges, man–made

noise and magnetospheric phenomena (such as chorus and hiss), where lightning discharges and man–made noise dominate. The low attenuation in this band allows the signals generated by lightning strokes, called atmospherics or sferics, to travel great distances around the earth. Thus, a lightning discharge above Africa can be easily detected by a receiver in North America. It is estimated that on average there are roughly 2000 thunderstorms active around the earth at any moment, generating an average of 100–200 lightning strokes/second. This lightning activity constitutes the major source of noise in the ELF range. Power line harmonics are a major source of man-made noise in the ELF , and their effect is evident throughout the whole frequency band in inhabited areas.

The background power spectrum in the ELF range is generally of the form $1/f^{\alpha}$ (Galejs [33],chapter 7), where α is typically close to 2. Maxwell [50] and Maxwell and Stone [51] show measurements of the background noise level at various location, and in [50] they discuss the dependence of the background noise spectrum on latitude. It is shown that the noise spectra correlate well with lightning spectra and propagation attenuation coefficients. The background noise varies with a period of 24 hours because of diurnal variations of global thunderstorm activity, and the seasonal variation of the noise is related to global thunderstorm activity. Gustafsson et al. [36] and Smith and Jenkins [80] present background level measurements recorded in northern latitudes, and demonstrate that the daytime background level is generally lower than the nighttime level. They suggest that the reason is enhanced ionospheric absorption during the day.

4 The Schumann Resonance

An interesting phenomenon in the lower end of the ELF band is the Schumann resonance, named after W. O. Schumann, who predicted it in 1952. The basic resonance mode (frequency 7.5 Hz) occurs when the wavelength of the propagating wave approximately equals the circumference of the earth (40,000 km). Constructive interference at the basic Schumann resonance and its harmonics results in an increased background noise level at these frequencies (figure 2).

Derivations of the Schumann resonance from general field expressions are

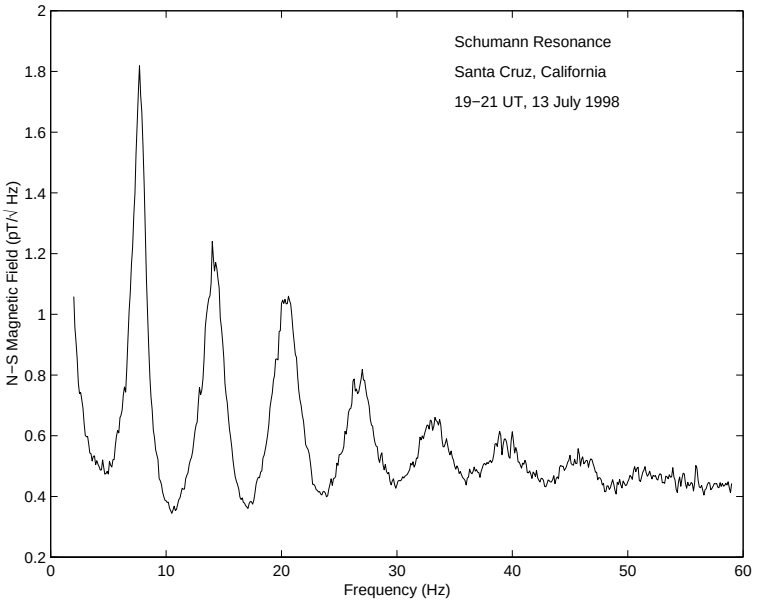

Figure 2: Spectrum of the first eight Schumann resonance modes. The basic resonance mode occurs when the wavelength approximately equals the circumference of the earth.

presented by Wait [85] and Jones [41], and extended by Large and Wait [48] to include the effects of the day/night inhomogeneity of the ionosphere. The Schumann resonance was first observed in 1960 by Balser and Wagner [5].

It is thought that the main source of energy for the Schumann resonance is lightning strokes occurring around the earth, and that, as a result, the resonance level is an indication of global lightning activity (Balser and Wagner [6], Nickolaenko et al. [57, 56], Ogawa et al. [60] and Heckman et al. [39]). The Schumann resonance is used to locate thunderstorms (Polk [68] and Galejs [32]), and to study the ionosphere (Sentman and Fraser [78]). Sao et al. [77] relate diurnal variations of the Schumann resonance frequency to solar ionizing radiation, solar zenith angle and geomagnetic disturbances.

The interest in the Schumann resonance was revived in the 1990s, when Williams [90] showed a correlation between the intensity of the first mode of the Schumann resonance and the fluctuations of the temperature in the tropical atmosphere. This suggests that the Schumann resonance can be used to monitor global climate changes. A recent summary on the Schumann resonance with many references is found in Nickolaenko [54].

5 Extension of the Waveguide Model

The modal theory of the earth–ionosphere waveguide is extended in this section from the simplified parallel–plate model with perfectly conducting walls, which was presented in section 1.

The extensions of the waveguide model presented here are:

- Consideration of the electrical properties of the earth and ionosphere and calculation of the reflection coefficients of the waveguide walls.
- Consideration of the spherical geometry of the earth, which imposes a spherical waveguide instead of a planar one.
- Consideration of the geomagnetic field, which causes anisotropic ionospheric reflections.

5.1 Reflection Coefficients

An accurate model of the earth–ionosphere waveguide for ELF wave propagation has to take into account the finite conductivities of the two limiting boundaries. The conductivity of the earth ranges from 10^{-4} S/m for dry rocky areas to 4 S/m for sea water, and the dielectric constant varies considerably as well. A list of the conductivity and the dielectric constant values of various types of soil and water is included in [38]. The earth is usually treated as a uniform sharp boundary, even though this model does not strictly apply to its changeable surface. The validity of the smooth earth model stems from the small scale of change of the surface, when compared to the long wavelengths involved in ELF propagation.

A further extension of the waveguide should take into account the inhomogeneity of the earth's surface conductivity. This extension of the waveguide theory is similar in nature to the theory related to ionospheric inhomogeneities discussed in section 8.

A realistic model of the ionosphere is more involved, since it depends on the concentration of free electrons and various positive ions, which in turn depend on complex generation mechanisms. Section 7 discusses the calculation of ionospheric reflection coefficients in more detail.

Another complication of the calculation of the ionospheric reflection coefficients stems from the fact that the ionospheric boundary is not sharp. In many cases, an 'effective height' is calculated for the waveguide model, and reflection is treated as though the ionosphere is sharply bounded at this height. Booker and Lefeuvre [16] calculate the effective ionospheric height for a simple profile of ionospheric ionization density, and show that it is frequency dependent. Greifinger and Greifinger [34] present a more complicated reflection model, which includes two ionospheric reflection layers at different heights.

The reflection coefficients of the earth and the ionosphere affect the eigenangles of the different modes. These in turn determine the attenuation that each mode undergoes and the relative amplitudes of the modes. The relation between the eigenangles of the different modes and the attenuation can be appreciated by

noting that if S_n is complex in equations (1), (2) and (4), then its imaginary part translates into attenuation through the exponential factor $e^{-ikS_n\rho}$. The effect of the reflection coefficients on the eigenangle can be appreciated by looking at the modal equation, shown here for the TM modes:

$$R_i(\omega,\theta_n)R_e(\omega,\theta_n)e^{-i2kh(\omega)C_n} = e^{-i2\pi n} \quad n = 0,1,2,\ldots \tag{9}$$

where $R_i()$ is the ionospheric reflection coefficient for TM waves, $R_e()$ is the earth reflection coefficient for TM waves, and $h(\omega)$ is the frequency dependent effective reflection height. Both reflection coefficients depend on the frequency ω and on the eigenangle θ_n.

5.2 Waveguide Geometry

The waveguide geometry affects the various modes (equations (1) and (4)). It has a minor effect on the modal equation (9), so the eigenangles are not strongly affected by the flat earth simplification.

When considering a spherical geometry rather than a parallel plate geometry, mode coupling is introduced. This means that TM waves propagating in the waveguide are partially converted to TE waves because of reflections from the curved walls of the waveguide (and conversely TE waves are converted to TM).

Expressions for the fields in a spherical waveguide are given by Wait [87], using a spherical coordinate system (r,θ,ϕ). The earth is modeled as a homogeneous sphere of radius a (=6370 km), conductivity σ_g and dielectric constant ϵ_g. The lower edge of the ionosphere is located at $r = a + h$, its conductivity is σ_i and its dielectric constant is ϵ_i. It is assumed that both the earth and the ionosphere are good but not necessarily perfect conductors. The source is a vertical electric dipole located at ground level at $r = a$, $\theta = 0$, $\phi = 0$ and the observation point is located on the ground at $r = a$, θ, $\phi = 0$ as in figure 3.

The vertical electric field in this configuration is

$$E_r = E_0\left(\frac{d/a}{\sin(d/a)}\right)^{1/2}\frac{(d/\lambda)^{1/2}}{(h/\lambda)}e^{i[2\pi(d/\lambda)-\pi/4]}\sum_{n=0}^{\infty}\delta_n S_n^{3/2}e^{-i2\pi S_n(d/\lambda)} \tag{10}$$

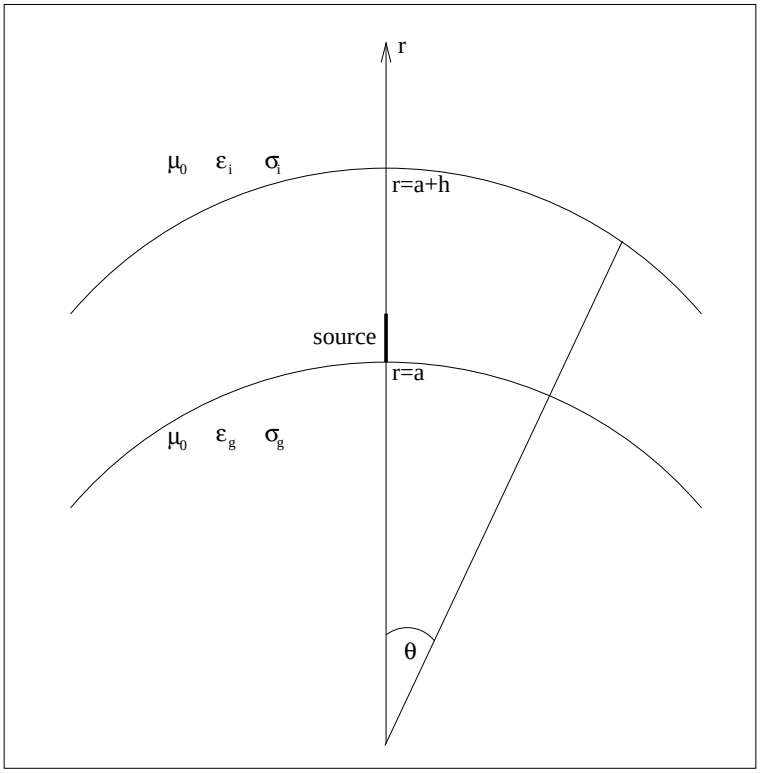

Figure 3: Geometry of the spherical earth–ionosphere waveguide with a spherical coordinate system.

where

λ is the free space wavelength,

$d = a\theta$ is the arc length between the source and the observer,

$\eta = \sqrt{\mu_0/\epsilon_0} \simeq 120\pi\ \Omega$ is the free space impedance,

E_0 is the field of the source at a distance d on a flat perfectly conducting earth.

For $d/\lambda \gg 1$

$$E_0 = -i(\eta/\lambda) I ds \frac{e^{-i2\pi d/\lambda}}{d} \tag{11}$$

$\delta_n \cong \begin{cases} \frac{1}{2} & n = 0 \\ 1 & n = 1, 2, \ldots \end{cases}$

$S_n = \sin\theta_n = \sqrt{1 - C_n^{1/2}}$ is the sine of the eigenangle of the n^{th} mode (which may be complex),

$C_n = \cos\theta_n$ is the cosine of the eigenangle of the n^{th} mode,

and θ_n is the eigenangle of the nth mode.

Equation (10) describes the field measured within the waveguide, for $a < r < a + h$. This expression is an approximation that is valid only if θ is not near 0 or π, which means that the source region and the antipode are excluded. The time dependence is $e^{i\omega t}$, where $\omega = \frac{2\pi c}{\lambda}$ is the angular frequency.

As the radius of the earth a tends to infinity, the flat earth approximation (eq. (1)) is recovered.

A first order approximation of the effect of the earth curvature on ELF fields is obtained by multiplying the field expressions in the parallel plate waveguide (eq. (1) and (4)) by the factor $1 + \frac{\theta^2}{12}$. The coordinate system used here is cylindrical, as in section 1.

$$E_z = \left(1 + \frac{\theta^2}{12}\right) E_0 \frac{(\rho/\lambda)^{1/2}}{(h/\lambda)} e^{i[k\rho - \pi/4]} \sum_{n=0}^{\infty} \delta_n S_n^{3/2} e^{-ikS_n\rho} \cos(kC_n z) \tag{12}$$

Using appropriate approximations, it can be shown that the field consists of two components. One of these components travels along the short great circle path connecting the source and the receiver, and the other travels along the complementary long great circle path, passing though the antipode (Wait [87]).

An interesting feature of the spherical waveguide is the antipodal concentration that causes the vertical electric field signals measured at the antipodal point to be stronger than signals measured at a similar distance away from the

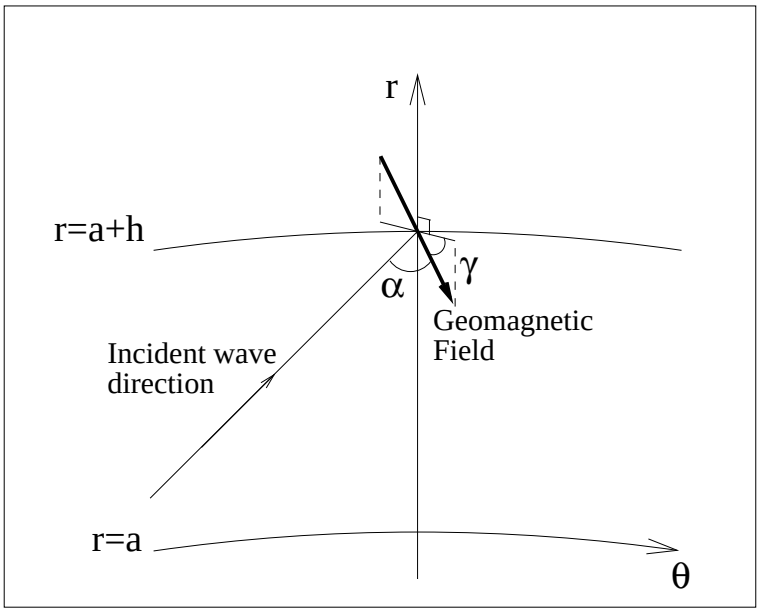

Figure 4: Geometry of the earth–ionosphere waveguide with the geomagnetic field present. γ is the direction of the geomagnetic field relative to the horizontal direction. α is the angle between the incident wave direction and the geomagnetic field.

source in a plane parallel waveguide. This effect is caused by the addition of many coherent signal components traveling along great circle paths between the source and the antipodal point. (The actual antipodal effect is more complex due to the day/night terminator (see section 8.1) and other propagation effects in the various paths.) The antipodal concentration and other antipodal effects are discussed further in section 6.

5.3 Geomagnetic Field

The static geomagnetic field affects the behavior of the ionospheric boundary of the waveguide. In the presence of the geomagnetic field, the ionosphere becomes anisotropic and the ionospheric reflection coefficient depends on the angle α between the incident wave front and the static magnetic field (see figure 4 for the definition of the angle α). This adds a new dependence to the ionospheric

reflection coefficient, further complicating the modal equation:

$$R_i(\omega, \theta_n, \alpha(\theta, \phi)) R_e(\omega, \theta_n) e^{-i2kh(\omega)C_n} = e^{-i2\pi n} \quad n = 0, 1, 2, \ldots \tag{13}$$

The direction and intensity of the geomagnetic field depend on the geomagnetic location and, as a result, the description of the earth–ionosphere waveguide has to take this location into account.

Dinger et al. [20] show that background noise measured in Norway at frequencies near 3 kHz is not isotropic. The east–west component of the measured noise (noise propagating along a east–west or west–east path) is 1–1.5 dB lower than the north–south component during the day, but increases around local sunset to a level of about 4 dB above the north–south component. The difference between noise levels measured in the two components is explained by the anisotropy of the propagation loss, which is caused by the geomagnetic field.

5.3.1 Non-reciprocity of ELF Propagation

The geomagnetic field introduces a directional dependence into the attenuation of ELF waves. This is the reason why ELF waves propagating west-to-east suffer higher attenuation than those propagating east-to-west in middle latitudes. This difference between the properties of the propagation between east–west and west–east paths is called the non-reciprocity of the propagation.

This effect is analyzed by Barr [11], who shows that the non-reciprocity is most notable for frequencies above 1 kHz. Barr [10] computes the attenuation factors for east-to-west and west-to-east propagation, and finds a difference of up to 45 dB/Mm. These results are shown to be in good agreement with measurements.

6 Antipodal Effects

Some fields measured at the antipodal point of a source are enhanced due to the spherical shape of the earth–ionosphere waveguide. The enhancement can be intuitively explained as the coherent addition of many waves traveling from the source to the antipodal point along great circle paths. Galejs [33] calculates

antipodal effects on the different field components generated by vertical and horizontal dipole sources. He shows that for a vertical dipole source the only field component present at the antipode is the vertical component of the electric field. For a horizontal dipole source the antipodal field contains horizontally directed electric and magnetic fields, perpendicular to each other, with the electric field parallel to the dipole axis. These results are also summarized in [31].

Wait [87] gives a brief description of antipodal effects for a vertical dipole source and shows that waves traveling through the antipode acquire a $\pi/2$ phase advance. Wait [86] and Jones [42] analyze the distortion of ELF pulses after propagation through an antipode. The $\pi/2$ phase advance of lightning–generated pulses traveling around the earth is examined.

Measurements of antipodal effects are difficult because of the long distances involved, which dictate the use of very strong sources. Measurements made on an 82 Hz signal are described in Fraser–Smith and Bannister [28]. The transmitting facility was located in north-western Russia and measurements showing antipodal concentration were made in New Zealand and Antarctica. Similar results, in the VLF band, are reported by Rogerson [76]. In this latter case the source was a U.S. Navy transmitter in Hawaii and the measurements were taken by an aircraft in the vicinity of the antipodal point located in southern Africa.

7 Ionospheric Reflection

This section describes the mechanism of reflection of ELF waves from the ionosphere. The ionosphere is conductive because it contains free electrons and positive ions, which are generated largely by solar UV and X radiation and by the precipitation of energetic charged particles from the magnetosphere. A discussion of the ionization generation mechanism and the various positive ions involved can be found in Richmond [73] and in other literature on the subject (Rees [72], Kato [44], Akasofu and Chapman [1], Ratcliffe [70, 69], Rishbeth and Garriot [75], Whitten and Poppoff [89] and Rawer [71]).

The amount of free charge in the ionosphere is determined by the equilibrium that is reached between the generation mechanisms and the recombination of the free electrons with the positive ions. The density of neutral particles in

the ionosphere exponentially decreases with altitude, which means that very little generation occurs in the high altitudes (above 500 km), where the particle density is low. The energetic particles precipitating from the magnetosphere gradually lose their energy as they penetrate the ionosphere, generating free charge as they travel downward. The solar radiation penetrating the ionosphere is likewise gradually absorbed while generating free charge in the ionosphere. The bottom of the ionosphere (around 50 km) is marked by very little generation of charge, because the ionizing radiation has lost most of its energy at higher altitudes. The density of free charge in the ionosphere is maximal at middle heights, where the generating mechanisms are strong and the density of particles is sufficient. The free electron density is maximal at an altitude of about 250 km above ground, with a few local maxima of density at lower altitudes. These local maxima of density constitute ionospheric layers with enhanced electron density, as seen in figure 5.

The layer about the altitude of 100 km is called the E layer, the layer at 170 km, which is sometimes absent at night, is the F_1 layer, and the top layer at 250 km is the F_2 or the F layer. The lowest layer, at about 70 km, is the D layer, which is almost always absent at night. A description of the structure and properties of the ionosphere is presented by Hargreaves [37].

The electron density height profile in the ionosphere differs greatly between day and night conditions, because of the different ionization generation rates driven by solar radiation. The electron density is also affected by solar activity, with the ionization being lowest during periods of low solar activity, as seen in figure 5.

The ionosphere is a plasma and its conductivity can be calculated using plasma theory, as described by Rishbeth and Garriot [75], Ratcliffe [70], and in other literature on the subject. The ionospheric plasma parameters (i.e. the types of particles and their concentrations) are altitude dependent, so the conductivity of the ionosphere also varies with altitude. In addition, the conductivity varies in the lateral plane, with the most notable variation occurring at the day/night terminator, which marks the dawn and dusk boundaries. Local disturbances in the ionosphere also cause lateral variations of the conductivity;

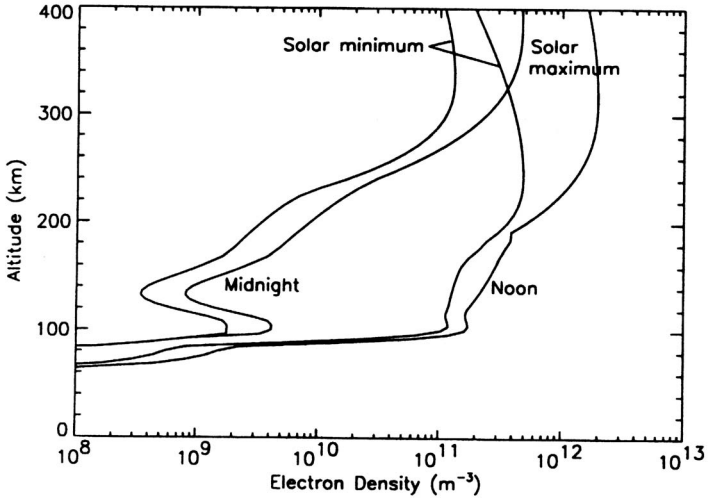

Figure 5: Typical electron densities at 44.6°N, 2.2°E at noon and midnight on March 21, for solar minimum and maximum conditions. The electron density determines the behavior of the ionospheric wall of the earth–ionosphere waveguide. Adapted from A. D. Richmond, in H. Volland (editor), 'Handbook of Atmospheric Electrodynamics', CRC Press 1995, with permission. (CRC Press Home Page http://www.crcpress.com).

these variations are discussed in section 8.

Due to the geomagnetic field, the ionosphere is an anisotropic conductor. The three most commonly used conductivities apply to specific directions relative to the geomagnetic field, as follows:

- The *Parallel Conductivity* σ_0 relates the current flowing along the static magnetic field with an electric field component in the same direction. This conductivity is not affected by the presence of the static magnetic field.

- The *Pederson Conductivity* σ_1 corresponds to current flowing in a perpendicular direction to the static magnetic field, when an electric field is applied in the same direction.

- The *Hall Conductivity* σ_2 corresponds to current flowing in a direction perpendicular to both the magnetic field and the electric field, when the electric field is perpendicular to the magnetic field.

Figure 6 shows typical mid–latitude vertical profiles of the daytime conductivity components for low solar activity. At altitudes above 80 km the parallel conductivity is much larger than the Pederson and Hall conductivities.

The reflection coefficients of the ionosphere depend on (a) the conductivity profile of the ionosphere, (b) the local geomagnetic field, (c) the direction of incidence, and (d) the polarization of the incident wave. Due to the complexity of the reflection coefficients, they are usually calculated numerically or empirically. Simplified empirical expressions of the reflection coefficients in day and night conditions are given in Volland [84] for a simplified model characterized by an exponential electron density and an exponential collision rate in the lower layers of the ionosphere. The effects of the geomagnetic field are neglected. The reflection coefficient for TM waves under these simplified conditions is

$$R_i \simeq e^{-(b_i - ic_i)/\cos\theta} \tag{14}$$

where b_i and c_i vary exponentially with frequency and θ is the incidence angle.

Harth [38] calculates the ionospheric reflection coefficient at 3 kHz using a thin layer method (see section 9 for a discussion of the thin layer method) with similar assumptions to Volland, and the results are presented graphically.

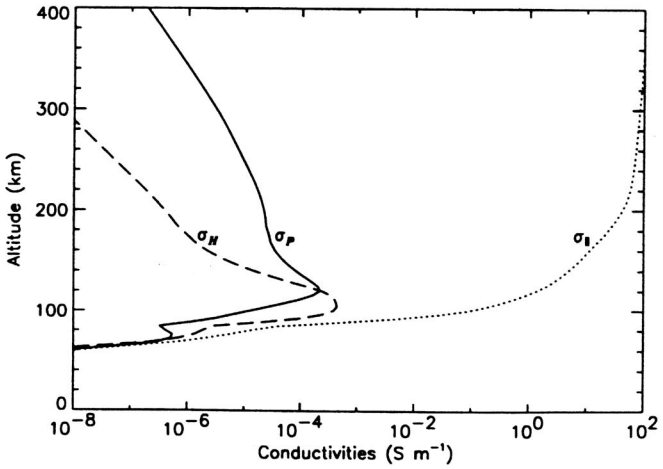

Figure 6: Typical noontime parallel (σ_0), Pedersen (σ_1) and Hall (σ_2) conductivities at 44.6°N, 2.2°E for solar minimum conditions on March 21. The different types of conductivity characterize the behavior of the ionosphere as a reflector of ELF waves. Adapted from A. D. Richmond, in H. Volland (editor), 'Handbook of Atmospheric Electrodynamics', CRC Press 1995, with permission. (CRC Press Home Page http://www.crcpress.com).

Wait and Spies [88] present graphs describing the reflection coefficient for an exponential electron density profile under various conditions. They show the effects of the magnetic field, angle of incidence, frequency, reflecting height and ground conductivity on the reflection coefficient. An experiment relating electron density profiles with VLF reflection coefficients is described by Mambo et at. [49].

A different approach to the calculation of the reflection coefficients is taken by Budden [17] who presents a plasma physics approach to understanding the ionosphere. The calculation of the refractive index and the characteristic polarization of waves traveling through the ionosphere is the basis of this approach. The admittance matrix of the ionosphere is calculated, which relates the horizontal components of the electric and magnetic field, and the reflection coefficients of the ionosphere are then derived from the matrix expressions. Two types of ionospheric boundaries are considered: A sharp boundary and a slowly varying one (Wentzel–Kramers–Brillouin (WKB) model). A similar approach is taken by Galejs [33], where the modal equations are presented in terms of the wave impedance rather than the reflection coefficient.

The ionosphere can usually be modeled as a sharp boundary for frequencies in the ELF range, since the wavelengths are large compared to the scales of length over which the ionospheric properties change. As a result, a simplified model of the ionosphere with a sharp bottom boundary is often sufficient.

8 The Inhomogeneous Ionosphere

A realistic picture of ELF propagation in the earth–ionosphere waveguide has to take into account the effects of inhomogeneities in the ionosphere. The vertical structure of the ionosphere, as represented by the ionospheric layers, was described in section 5.1. The following section describes the effects of the lateral structures and variations in the ionosphere on ELF propagation.

The lateral structure of the ionosphere and various inhomogeneities affect the propagation loss in the ELF range, and some affect the propagation path. However, when compared to other frequency bands, propagation in the ELF

band appears more stable under ionospheric disturbances.

8.1 Day/Night Terminator Effect

The line marking the transition between day and night is named the 'day/night terminator', or simply the 'terminator', and the transition has a profound effect on propagating ELF radiation. Measurements show that the phase velocity of ELF waves traveling across the day/night terminator can be approximated as a weighted average of day and night phase velocities, with each velocity given a weight according to the length of the path in the two regions (Hughes and Gallenberger [40]). The loss in mixed day/night paths varies in a more complex manner with the percentage of the sunlit section in the path. Measurements at 400 Hz show deep fades when the night–day terminator is located above the receiver (Davis [18]), which are not explained by a smooth transition between day and night regions.

ELF waves are also reflected from the day/night terminator. Bezrodnyi et al. [15] measure a reflection coefficient for VLF signals using the Doppler shift produced by the terminator motion. Their measurements show that the reflection coefficient is on the order of 10^{-2}–10^{-3}. Field and Joiner [26] calculate the lateral refection and transmission coefficients of ELF transverse electromagnetic (TEM) waves from the terminator.

Theoretical analysis of the effects of the terminator on ELF propagation is given by Nikolaenko [59] and by Field and Joiner [26]. Nikolaenko [59] calculates the effect of the terminator in three geometrical arrangements, describing different directions of wave propagation relative to the terminator (parallel, perpendicular and inclined). Figure 7 shows the perturbation in the vertical electric field from the homogeneous ionosphere model for an inclined propagation path relative to the terminator.

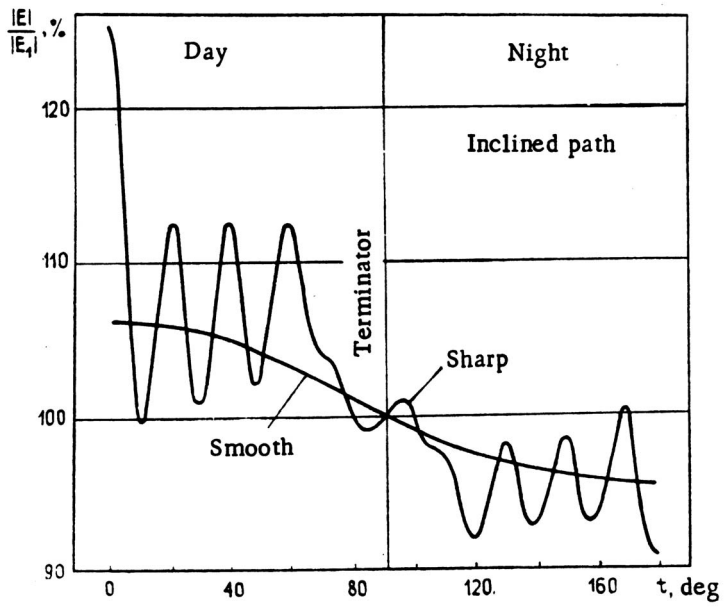

Figure 7: Amplitude of the vertical electric field in a propagation path inclined 45° from the terminator, relative to the unperturbed field in the models of the smooth and sharp terminators. The day/night terminator is the main source of lateral variation in the earth–ionosphere waveguide. Adapted from A. P. Nikolaenko, in Radiophysics and Quantum Electronics, Vol 29, No.1, Plenum Publishing Corporation 1986, with permission.

8.2 Ionospheric Disturbances

8.2.1 Varieties of Disturbances

Three major varieties of ionospheric disturbances are: (1) sudden ionospheric disturbances (SID), (2) magnetic storms, and (3) solar proton events (SPE), also named proton storms [75]. They can be defined as follows:

- *Sudden Ionospheric Disturbances* (SID) are related to solar flares, electromagnetic phenomena which enhance the electron density of the D region by up to a factor of ten.
- *Magnetic Storms* are caused by enhancements of the solar wind, a stream of particles traveling away from the sun. An increase in the particle concentration of the solar wind, accompanied by an increase in their velocity causes ionospheric modifications where it reaches the magnetosphere, which result in magnetic storms.
- *Solar Proton Events* (SPE) are caused by energetic streams of solar protons (accompanied by electrons). On arrival at the earth the protons are deviated by the geomagnetic field and they impinge on the polar caps, so solar proton events are related to polar cap absorption (PCA) events.

Other ionospheric disturbances include the effect of sporadic E layers and small scale ionospheric irregularities. A summary of ionospheric disturbances and their effect on radio propagation is given by Hargreaves [37].

8.2.2 General Considerations

The theoretical analysis of ionospheric inhomogeneities often involves calculations of the electromagnetic field scattered from the inhomogeneities. Pappert [64] calculates the field scattered from a cylindrically symmetric ionospheric disturbance and compares the expected effect of disturbed polar cap boundaries to measurements. The cylindrically symmetric ionospheric disturbance model is also useful in describing small scale ionospheric irregularities.

The effect of local ionospheric disturbances on ELF propagation is analyzed by Nickolaenko [53, 58] using a perturbation theory. The disturbances analyzed are local variations of the electrical properties of the ionosphere, and changes in the effective ionospheric reflection height. The analysis shows that the effects of these two types of disturbances on ELF propagation are similar and that the effect of local disturbances is greatest when the irregularity is situated above the source or the observer.

Random distortions in ionospheric height and fluctuations of electrical properties cause fluctuations of ELF waves propagating in the earth–ionosphere waveguide; these are analyzed by Kostigov [46] using a perturbation method.

8.2.3 Specific Effects

Ionospheric inhomogeneous phenomena affect ELF waves traveling between the ionosphere and the earth. Bannister [8] reviews measurements of various ELF propagation phenomena related to ionospheric irregularities, some of which are mentioned below.

The effects of sudden ionospheric disturbances caused by solar flares on ELF propagation are analyzed by Field [24], and the resulting modal attenuation coefficients are compared to measurement. The X–ray radiation associated with solar flares causes a lowering of the D layer, which reduces the propagation loss in the ELF range relative to non-disturbed conditions.

Precipitation of energetic electrons in the several days following magnetic storms may cause enhanced loss in the ELF range at night. Measurements showing this effect are described by Davis [19] and Bannister [8], but the theoretical explanation is incomplete. Three different groups analyzed a magnetic storm that occurred in December 1971 using satellite measurements, and all of them measured enhanced electron precipitation and enhanced levels of ELF radiation (Parady and Cahill [67], Vakulov et al. [82] and Kovner et al. [47]). These results suggest that the relationship between the electron precipitation and the ELF fields is connected with the location of the magnetopause, i.e. the outer termination of the geomagnetic field.

Occasional night time decreases in ELF signal levels may be explained by the presence of sporadic E layers (Bannister [7, 8]). The measurements described by Bannister include ELF anomalies at two different locations, appearing 2–4 hours apart, which may be the result of a traveling sporadic E layer. Further analysis of the measurements from these two locations yield an estimate of the velocity and path of the sporadic E layer (Pappert [63]).

Theoretical analyses of the effect of sporadic E layers on ELF propagation are given by Pappert [62] and by Pappert and Moler [66]. Their results indicate that a sporadic E layer 1 Mm by 1 Mm may cause 6-8 dB attenuation in the ELF range. Patches 1 Mm by 0.5 Mm can account for fades in the 3–4 dB range. The deepest fades require the center of the disturbance to be close either to the source or to the receiver, but large patches cause significant attenuation at distances of up to 10 Mm from the direct propagation path between the source and receiver.

The main effect of a solar proton event (SPE) is an increase in the attenuation in the ELF range for paths passing near the boundary of the polar cap (Katan and Bannister [43], Field et al. [27] and Fraser–Smith and Helliwell [29]). The additional attenuation may be caused by lateral refraction, which bends the signal path away from the polar cap boundary and into the central cap zone. Field et al. [27] predict enhanced field levels inside the polar cap boundary, but this was not verified by measurement.

The expected effects of nuclear events on ELF propagation via ionospheric changes is surveyed by Bannister [8].

9 ELF Calculation Methods

This section describes the approaches used to calculate ELF fields in the earth–ionosphere waveguide. As already indicated, an accurate representation of the earth-ionosphere waveguide is extremely complex, and calculations are often done numerically, incorporating information about various ionospheric and ground parameters.

The two main computational approaches presented here, namely (a) the full–

wave approach and (b) the thin layer approach, are suitable for a horizontally stratified ionosphere with no lateral variation. Calculation methods for laterally varying ionospheres are also surveyed.

A non–iterative approximate method for calculating eigenvalues of the ELF modes, based on a two–layer ionospheric model, is presented by Greifinger and Greifinger [34] and elaborated in [35]. The physical significance of a reflecting layer for ELF waves within the ionosphere is discussed in these papers.

9.1 The Full–Wave Approach

The full–wave approach involves the numerical integration of four coupled first–order complex differential equations containing an eigenvalue parameter (Greifinger and Greifinger [35]). The calculated quantity may be (a) the components of the electromagnetic field, (b) ratios of field component, which may represent impedances, and (c) reflection coefficients. The full–wave integration starts from the top of the ionosphere, where propagation is assumed to be upward only. An initial value of propagation parameters is assumed at this height. Integration is performed downward along a vertical path, and boundary conditions are checked at the surface of the earth. Inconsistencies of the boundary conditions at the surface of the earth lead to corrections of the initial value (of propagation parameters at the top of the ionosphere), and the whole process repeats with new initial values, until the boundary conditions are matched to some chosen accuracy.

A full–wave calculation of the ionospheric reflection coefficients is described by Pappert and Moler [65]. The ionosphere is assumed to vary slowly along the lateral propagation path, and the WKB approximation is used.

Field [23] uses a full–wave method to calculate the ionospheric wave admittance for normal and disturbed ionospheric conditions, and calculates the fields within the waveguide.

Aksenov and Nazarova [2] use a full-wave method to calculate the dependence of ionospheric reflection and transmission coefficients on the angle of incidence, frequency and geomagnetic field for ionospheric models of the day and night.

9.2 The Thin Layer Approach

The thin layer approach is similar in principle to the full–wave approach, but the ionosphere is taken to be a collection of thin homogeneous layers, rather then a continuum. The process is started with some initial values of the parameters at the top boundary of the ionosphere, and then the boundary conditions are matched between adjacent layers, going downward until a lower boundary is reached. The thin layer method is iterative in a similar way to the full-wave method: the boundary conditions at the lower boundary are used to correct the initial values, and the calculation process is repeated until convergence is achieved to a desired accuracy.

Galejs [30] presents a thin layer method, where the surface impedance computed at a lower boundary is used to correct the initial conditions. The field components are calculated for each layer, and from these the wave impedances are derived. This procedure is used to calculate the frequency dependent attenuation rate for day and night conditions and to examine the effect of the anisotropy of the ionosphere.

A similar approach is presented by Altman and Cory [4, 3], where the ionosphere is treated as a collection of discrete layers and an iterative process is used to calculate ELF propagation parameters, each iteration starting from the top of the ionosphere. This method is presented as a derivation from the thin–film method used in optics.

Another thin layer method is presented by Nagano et al. [52], where the calculated quantities are the components of the field. Nagano et al. [52] compare the width of the layers required for their method to the step size required in various full–wave methods and show that their thin layer method produces comparable results to full–wave methods, with much bigger step sizes. The complexity (computer time) of the two methods is also compared, and it is shown that the thin layer method is more efficient.

9.3 Lateral Variations in the Waveguide

Lateral variations in the earth–ionosphere waveguide may be treated by the WKB approach, which assumes slow variation in the waveguide. However, this

approach is of little use in the ELF band, because the wavelengths involved are very large with the result that in many cases the ionospheric or ground variations are not slow when compared to the wavelength.

An important approach to lateral variations in the waveguide is based on an integral equation describing the lateral propagation (Field and Joiner [25]). The integral equation is solved numerically in terms of the sine of the eigenangle. This approach is based on the simplified assumptions that vertical variations in the ionosphere are decoupled from lateral variations and that lateral variations are much slower than vertical variations. A program which predicts vertical ELF fields in an inhomogeneous waveguide is described by Ferguson et al. [21]. This program uses the moment method to solve the integral equation numerically.

Another approach to the laterally varying waveguide is based on ray theory, where vertical inhomogeneities are assumed to be uncoupled from the lateral variations. The vertical inhomogeneities are usually treated in a full-wave approach, and the lateral variations are treated using ray theory. Field et al. [27] use the full–wave/ray method to analyze the effects of polar cap absorption events on ELF propagation.

A calculation of the electric field, given the eigenvalues of the propagation, is described by Shellman [79]. The method is based on the knowledge of the sine of the waveguide eigenangle at elements of a mesh point array that extends around the earth. The lateral variation of the waveguide is described by the eigenvalues at different locations.

Acknowledgments

The authors thank Martin Füllekrug for the Schumann resonance data plotted in figure 2.

This work was supported in part by the Office of Naval Research through Grant N00014-92-5-1576.

References

[1] S. I. Akasofu and S. Chapman. *Solar-Terrestrial Physics*. Clarendon, Oxford, 1972.

[2] V. I. Aksenov and M. V. Nazarova. Numerical solution of the problem of transmission of ELF waves through the lower ionosphere. *Radio Engineering and Electronic Physics*, 17(7):1057–1064, 1972.

[3] C. Altman and H. Cory. The generalized thin-film optical method in electromagnetic wave propagation. *Radio Science*, 4(5):459–470, May 1969.

[4] C. Altman and H. Cory. The simple thin-film optical method in electromagnetic wave propagation. *Radio Science*, 4(5):449–457, May 1969.

[5] M. Balser and C. A. Wagner. Observations of earth-ionosphere cavity resonances. *Nature*, 188:638–641, November 1960.

[6] M. Balser and C. A. Wagner. Diurnal power variations of the earth-ionosphere cavity modes and their relationship to worldwide thunderstorm activity. *Journal of Geophysical Research*, 67(2):619–625, February 1962.

[7] P. R. Bannister. Localized ELF nocturnal propagation anomalies. *Radio Science*, 17(3):627–634, May-June 1982.

[8] P. R. Bannister. ELF propagation update. *IEEE Journal of Oceanic Engineering*, OE-9(3):179–188, July 1984.

[9] P. R. Bannister. Simplified formulas for ELF propagation at shorter distances. *Radio Science*, 21(3):529–537, May-June 1986.

[10] R. Barr. The propagation of ELF and VLF radio waves beneath an inhomogeneous anisotropic ionosphere. *Journal of Atmospheric and Terrestrial Physics*, 33:343–353, 1971.

[11] R. Barr. Some new features of ELF attenuation. *Journal of Atmospheric and Terrestrial Physics*, 34:411–420, 1972.

[12] R. Barr, M. T. Rietveld, P. Stubbe, and H. Kopka. Ionospheric heater bean scanning: A mobile source of ELF radiation. *Radio Science*, 22(6):1073–1083, November 1987.

[13] R. Barr and P. Stubbe. ELF and VLF radiation from the "polar electrojet antenna". *Radio Science*, 19(4):1111–1122, July-August 1984.

[14] R. Barr, P. Stubbe, M. T. Rietveld, and H. Kopka. ELF and VLF signals radiated by the "polar electrojet antenna": experimental results. *Journal of Geophysical Research*, 91(A4):4451–4459, April 1986.

[15] V. G. Bezrodnyi, P. V. Bliokh, I. S. Fal'kovich, and Yu. M. Yampol'skii. Reflection of superlong waves from the terminator in the earth-ionosphere waveguide. *Radiophysics and Quantum Electronics*, 21(11):1100–1114, November 1978.

[16] H. G. Booker and F. Lefeuvre. The relation between ionospheric profiles and ELF propagation in the earth-ionosphere transmission line. *Journal of Atmospheric and Terrestrial Physics*, 39:1277–1292, 1977.

[17] K. G. Budden. *The Propagation of Radio Waves.* Cambridge university Press, 1985.

[18] J. R. Davis. ELF propagation irregularities on northern and mid-latitude paths. In J. A. Holtet, editor, *ELF-VLF Radio Wave Propagation Proceedings of the NATO Advanced Study Institute, April 17-27 1974*, pages 263–277, Dordrecht, Boston, USA, 1974. D. Riedel Publishing Company.

[19] J. R. Davis. Localized nighttime D-region disturbances and ELF propagation. *Journal of Atmospheric and Terrestrial Physics*, 38:1309–1317, 1976.

[20] R. J. Dinger, W. D. Meyers, and J. R. Davis. Experimental investigation of ambient electromagnetic noise from 1.0 to 4.0 kHz in Italy and Norway. *Radio Science*, 17(1):285–302, January-February 1982.

[21] J. A. Ferguson, L. R. Hitney, and R. A. Pappert. A program to compute vertical electric ELF fields in a laterally inhomogeneous earth-ionosphere waveguide. Technical Report NOCS TR 851, Naval Ocean Systems Center, San Diego, CA, USA, December 1982.

[22] A. J. Ferraro, H. S. Lee, T. W. Collins, M. Baker, D. Werner, F. M. Zain, and P. J. Li. Measurements of extremely low frequency signals from modulation of the polar electrojet above Fairbanks, Alaska. *IEEE Transactions on Antennas and Propagation*, 37(6):802–805, June 1989.

[23] E. C. Field. Propagation of ELF waves under normal and naturally disturbed conditions. *Journal of Geophysical Research*, 74(14):3639–3650, July 1969.

[24] E. C. Field. VLF and ELF propagation during sudden ionospheric disturbances. *Journal of Geophysical research*, 75(10):927–33, April 1970.

[25] E. C. Field and R. G. Joiner. An integral-equation approach to long-wave propagation in a nonstratified earth-ionosphere waveguide. *Radio Science*, 14(6):1057–1068, November-December 1979.

[26] E. C. Field and R. G. Joiner. Effects of lateral ionospheric gradients on ELF propagation. *Radio Science*, 17(3):693–700, May-June 1982.

[27] E. C. Field, C. R. Warber, and R. G. Joiner. Effects of the ionosphere on ELF signals during polar cap absorption event: comparison of theory and experiments. In H. Soicher, editor, *AGARD Conference Proceedings No. 382 Propagation Effects on Military Systems in the High Latitude Region*, pages 8.3–1–8.3–10. North Atlantic Treaty Organization, 1985.

[28] A. C. Fraser-Smith and P. R. Bannister. Reception of ELF signals at antipodal distances. *Radio Science*, 33(1):83–88, January-February 1998.

[29] A. C. Fraser-Smith and R. A. Helliwell. ELF sferic occurrences in the antarctic during a solar proton event: case study of occurrences at Byrd station during the event of june 9, 1968. *Journal of Geophysical Research*, 85(A5):2296–2306, May 1980.

[30] J. Galejs. On the terrestrial propagation of ELF and VLF waves in the presence of a radial magnetic field. *Radio Science Journal of Research NBS/USNC-URSI*, 69D(5):705–720, May 1965.

[31] J. Galejs. Near fields and antipodal fields in the terrestrial earth-ionosphere waveguide. *Proceedings of the IEE*, 116(7):1150–1158, July 1969.

[32] J. Galejs. Frequency variations of Schumann resonances. *Journal of Geophysical Research*, 75(16), June 1970.

[33] J. Galejs. *Terrestrial Propagation of Long Electromagnetic Waves*. Pergamon Press, Oxford, New York, USA, first edition, 1972.

[34] C. Greifinger and P. Greifinger. Approximate method for determining ELF eigenvalues in the earth-ionosphere waveguide. *Radio Science*, 13(5):831–837, September-October 1978.

[35] C. Greifinger and P. S. Greifinger. Noniterative procedure for calculating ELF mode constants in the anisotropic earth-ionosphere waveguide. *Radio Science*, 21(6):981–990, November-December 1986.

[36] G. Gustafsson, A. Egeland, and J. Aarons. Audio-frequency electromagnetic radiation in the auroral zone. *Journal of Geophysical Research*, 65(9):2749–2758, September 1960.

[37] J. K. Hargreaves. *The solar-terrestrial environment*. Cambridge atmospheric and space science series. Cambridge University Press, 1992.

[38] W. Harth. Theory of low frequency wave propagation. In H. Volland, editor, *CRC Handbook of Atmospherics*, volume II, pages 133–202. CRC Press, Boca Raton, Fla., USA, 1982.

[39] S. J. Heckman, E. Williams, and B. Boldi. Total global lightning inferred from Schumann resonance measurements. *Journal of Geophysical Research*, 103(D24):31,775–31,779, December 1998.

[40] H. G. Hughes and R. J. Gallenberger. Propagation of extremely low-frequency (ELF) atmospherics over a mixed day-night path. *Journal of Atmospheric and Terrestrial Physics*, 36:1643–1661, 1974.

[41] D. L. Jones. Numerical computations of terrestrial ELF electromagnetic wave fields in the frequency domain. *Radio Science*, 5(5):803–809, 1970.

[42] D. L. Jones. Propagation of ELF pulses in the earth-ionosphere cavity and application to 'slow tail' atmospherics. *Radio Science*, 5(8,9):1153–1162, 1970.

[43] J. R. Katan and P. R. Bannister. Summary of ELF propagation variations at mid and high latitudes during the November/December 1982 and February 1984 solar proton events. *Radio Science*, 22(1):111–124, January-February 1987.

[44] S. Kato. *Dynamics of the Upper Atmosphere*. D. Reidel, 1980.

[45] F. J. Kelly. ELF/VLF/LF propagation and system design. Technical Report NRL Report 9028, Naval Research Laboratory, June 1987.

[46] K. I. Kostigov. Theory of fluctuations of super-long radio waves caused by random deformations of the boundaries of the earth surface – ionosphere waveguide channel. *Radio Engineering and Electronic Physics*, 19(8):123–126, August 1974.

[47] M. S. Kovner, V. A. Kuznetsova, V. I. Larkinna, and Ya. I. Likhter. High-energy electron flux and ELF radiation flux at ionospheric heights during the magnetic storm of December 16, 1971. *Cosmic Research*, 15(3):374–379, May-June 1977.

[48] D. B. Large and J. R. Wait. Theory of electromagnetic coupling phenomena in the earth-ionosphere cavity. *Journal of Geophysical Research*, 73(13):4335–4362, July 1968.

[49] M. Mambo, I. Nagano, S. Okada, and T. Fukami. An improved method of estimating electron density profiles in the lower ionosphere with VLF reflec-

tion coefficients. *Electronics and Communications in Japan*, 67-B(7):28–37, 1984.

[50] E. L. Maxwell. Atmospheric noise from 20 Hz to 30 kHz. *Radio Science*, 2(6):637–644, June 1967.

[51] E. L. Maxwell and D. L. Stone. Natural noise fields from 1 cps to 100 kc. *IEEE Transactions on Antennas and Propagation*, pages 339–343, May 1963.

[52] I. Nagano, M. Mambo, and G. Hutatsuishi. Numerical calculation of electromagnetic waves in an anisotropic multilayered medium. *Radio Science*, 10(6):611–617, June 1975.

[53] A. P. Nickolaenko. ELF radio wave propagation in a locally nonuniform earth-ionosphere cavity. *Radio Science*, 29(5):1187–1199, September-October 1994.

[54] A. P. Nickolaenko. Modern aspects of Schumann resonance studies. *Journal of Atmospheric and Solar-Terrestrial Physics*, 59(7):805–816, 1997.

[55] A. P. Nickolaenko and M. Hayakawa. Natural electromagnetic pulses in the ELF range. *Geophysical Research Letters*, 25(16):3103–3106, August 1998.

[56] A. P. Nickolaenko, M. Hayakawa, and Y. Hobara. Temporal variations of the global lightning activity deduced from the Schumann resonance data. *Journal of Atmospheric and Terrestrial Physics*, 58(15):1699–1709, 1996.

[57] A. P. Nickolaenko and L. M. Rabinowicz. Study of the annual changes of global lightning distribution and frequency variations of the first Schumann resonance mode. *Journal of Atmospherics and Terrestrial Physics*, 57(11):1345–1348, 1995.

[58] A. P. Nikolaenko. Effects of a local inhomogeneity in the ionosphere on the propagation of ELF radio waves. *Radiophysics and Quantum Electronics*, 27(10):856–864, October 1984.

[59] A. P. Nikolaenko. Scattering of ELF radio waves on global inhomogeneities of the earth-ionosphere cavity. *Radiophysics and Quantum Electronics*, 29(1):26–32, January 1986.

[60] T. Ogawa, Y. Tanaka, and M. Yasuhara. Schumann resonances and worldwide thunderstorm activity. In S. C. Coroniti and J. Hughes, editors, *Planetary Electrodynamics*, volume 2, chapter V-7. Gordon and Breach Science Publishers, New York, NY, USA, 1969.

[61] K. Papadopoulos, C. L. Chang, P. Vitello, and A. Drobot. On the efficiency of ionospheric ELF generation. *Radio Science*, 25(6):1311–1320, November-December 1990.

[62] R. A. Pappert. Effects of a large patch of sporadic-E on night-time propagation at lower ELF. *Journal of Atmospheric and Terrestrial Physics*, 42:417–425, 1980.

[63] R. A. Pappert. Calculated effects of traveling sporadic E on nocturnal ELF propagation: Comparison with measurement. *Radio Science*, 20(2):229–246, March-April 1985.

[64] R. A. Pappert. ELF scattering in the earth-ionosphere waveguide. *Radio Science*, 24(5):629–639, September-October 1989.

[65] R. A. Pappert and W. F. Moler. Propagation theory and calculations at lower extremely low frequencies (ELF). *IEEE Transactions on Communications*, COM-22(4):438–451, April 1974.

[66] R. A. Pappert and W. F. Moler. A theoretical study of ELF normal mode reflection and absorption produced by night-time ionospheres. *Journal of Atmospheric and Terrestrial Physics*, 40:1031–1045, 1978.

[67] B. Parady and L. J. Cahill Jr. ELF observations during the December 1971 storm. *Journal of Geophysical Research*, 78(22):4765–4770, August 1973.

[68] C. Polk. Relation or ELF noise and Schumann resonances to thunderstorm activity. In S. C. Coroniti and J. Hughes, editors, *Planetary Electrody-*

namics, volume 2, chapter V-6, pages 55–83. Gordon and Breach Science Publishers, New York, NY, USA, 1969.

[69] J. A. Ratcliffe. *Sun, Earth and Radio*. McGraw-Hill Book Company, 1970.

[70] J. A. Ratcliffe. *An Introduction to the Ionosphere and Magnetosphere*. Cambridge the University Press, 1972.

[71] K. Rawer. *The Ionosphere; Its Significance for Geophysics and Radio Communications*. F. Ungar Publishing Co., New York, 1957. Translated from German by L. Katz.

[72] M. H. Rees. *Physics and Chemistry of the Upper Atmosphere*. Cambridge University Press, 1989.

[73] A. D. Richmond. The ionospheric wind dynamo: effects of its coupling with different atmospheric regions. In R. M. Johnson and T. L. Killeen, editors, *The upper Mesosphere and Lower Thermosphere*. American Geophysical Union, Washington, DC, USA, 1995.

[74] M. T. Rietveld, R. Barr, H. Kopka, E. Nielsen, P. Stubbe, and R. L. Dowden. Ionospheric heater beam scanning: A new technique for ELF studies of the auroral ionosphere. *Radio Science*, 19(4):1069–1077, July-August 1984.

[75] H. Rishbeth and O. K. Garriot. *Introduction to Ionospheric Physics*. Academic Press, 1969.

[76] J. E. Rogerson. Airborne field strength measurements in the region of the NPM antipode. *Radio science*, 2(6):581–587, June 1967.

[77] K. Sao, M. Yamashita, S. Tanahashi, H. Jindoh, and K. Ohta. Experimental investigations of Schumann resonance frequencies. *Journal of Atmospheric and Terrestrial Physics*, 35:2047–2053, 1973.

[78] D. D. Sentman and B. J. Fraser. Simultaneous observations of Schumann resonances in California and Australia: Evidence for intensity modulation

by the local height of the D region. *Journal of Geophysical Research*, 96(A9):15,973–15,984, September 1991.

[79] C. H. Shellman. A model for propagation of ELF waves throughout the lateral extent of the inhomogeneous earth-ionosphere waveguide. *Radio Science*, 24(1):35–46, January-February 1989.

[80] A. J. Smith and P. J. Jenkins. A survey of natural electromagnetic noise in the frequency range f=1-10kHz at Halley station, Antarctica: 1. radio atmospherics from lightning. *Journal of Atmospheric and Solar-Terrestrial Physics*, 60(2):263–277, 1998.

[81] P. Stubbe, H. Kopka, M. T. Rietveld, A. Frey, P. Høeg, H. Kohl, E. Nielsen, G. Rose, C. LaHoz, R. Barr, H. Derblom, Å. Hedberg, B. Thidé, T. B. Jones, T. Robinson, A. Brekke, T. Hansen, and O. Holt. Ionospheric modification experiments with the Tromsø Heating Facility. *Journal of Atmospheric and Terrestrial Physics*, 47(12):1151–1163, 1985.

[82] P. V. Vakulov, Yu. Dubinski, A. V. Zahkarov, K. Kudela, S. N. Kuznetsov, V. A. Kuznetsova, V. I. Larkina, Ya. I. Likhter, S. Fisher, and I. A. Yuzefovich. Spilling of charged particles from the radiation belts and variations in the intensity of the ELF radiation in the recovery phase of the magnetic storm of December 16-17, 1971. *Cosmic research*, 12(5):645–652, September-October 1974.

[83] J. Villaseñor, A. Y. Wong, B. Song, J. Pau, and M. McCarrick. Comparison of ELF/VLF generation modes in the ionosphere by the HIPAS heater array. *Radio Science*, 31(1):211–226, January-February 1996.

[84] H. Volland. Longwave sferics propagation within the atmospheric waveguide. In H. Volland, editor, *Handbook of Atmospheric Electrodynamics*, volume II, chapter 3, pages 65–93. CRC Press, Boca Raton, Fla., USA, 1995.

[85] J. R. Wait. Earth-ionosphere cavity resonances and the propagation of ELF radio waves. *Radio Science*, 69D(8):1057–1070, August 1965.

[86] J. R. Wait. Distortion of an ELF pulse after propagation through an antipode. *Journal of Geophysical Research*, 74(11):2982–2986, June 1969.

[87] J. R. Wait. *Electromagnetic Waves in Stratified Media*. Pergamon Press, Oxford, New York, USA, 1970. Revised Edition Including Supplemented Material.

[88] J. R. Wait and K. P. Spies. Characteristics of the earth-ionosphere waveguide for VLF radio waves. Technical Note 300, National Bureau of standards, December 1964.

[89] R. C. Whitten and I. G. Poppoff. *Physics of the Lower Ionosphere*. Prentice-Hall Inc. Engelwood Cliffs, NJ, 1965.

[90] E. R. Williams. The Schumann resonance: a global tropical thermometer. *Science*, 256:1184–1187, May 1992.